Variational and parquet-diagram calculations for neutron matter. II. Twisted chain diagrams

E. Krotscheck [1] and J. Wang [2]
[1]*Department of Physics, University at Buffalo, SUNY Buffalo New York 14260, USA*
[2]*Institut für Theoretische Physik, Johannes Kepler Universität, A 4040 Linz, Austria*

(Received 22 September 2020; accepted 12 November 2020; published 3 December 2020)

We develop a manifestly microscopic method to deal with strongly interacting nuclear systems that have different interactions in spin-singlet and spin-triplet states. In a first step we analyze variational wave functions that have been suggested to describe such systems and demonstrate that the so-called commutator contributions can have important effects whenever the interactions in the spin-singlet and the spin-triplet states are very different. We then identify these contributions as terms that correspond, in the language of perturbation theory, to non-parquet diagrams. We include these diagrams in a way that is suggested by the Jastrow-Feenberg approach and show that the corrections from non-parquet contributions are, at short distances, larger than all other many-body effects.

DOI: 10.1103/PhysRevC.102.064305

I. INTRODUCTION

Popular models of the nucleon-nucleon forces [1–5] represent the interaction as a sum of local functions times correlation operators, i.e.,

$$\hat{v}(i,j) = \sum_{\alpha=1}^{n} v_\alpha(r_{ij})\,\hat{O}_\alpha(i,j), \tag{1.1}$$

where $r_{ij} = |\mathbf{r}_i - \mathbf{r}_j|$ is the distance between particles i and j and the $O_\alpha(i,j)$ are operators acting on the spin, isospin, and possibly the relative angular momentum variables of the individual particles. According to the number of operators n, the potential model is referred to as a $\hat{v}_n$ model potential. Semirealistic models for nuclear matter keep at least the six base operators and these are

$$\begin{aligned}
\hat{O}_1(i,j;\hat{\mathbf{r}}_{ij}) &\equiv \hat{O}_c = \mathbb{1},\\
\hat{O}_3(i,j;\hat{\mathbf{r}}_{ij}) &\equiv \boldsymbol{\sigma}_i\cdot\boldsymbol{\sigma}_j,\\
\hat{O}_5(i,j;\hat{\mathbf{r}}_{ij}) &\equiv S_{ij}(\hat{\mathbf{r}}_{ij}) \equiv 3(\boldsymbol{\sigma}_i\cdot\hat{\mathbf{r}}_{ij})(\boldsymbol{\sigma}_j\cdot\hat{\mathbf{r}}_{ij}) - \boldsymbol{\sigma}_i\cdot\boldsymbol{\sigma}_j,\\
\hat{O}_{2n}(i,j;\hat{\mathbf{r}}_{ij}) &= \hat{O}_{2n-1}(i,j;\hat{\mathbf{r}}_{ij})\boldsymbol{\tau}_1\cdot\boldsymbol{\tau}_2,
\end{aligned} \tag{1.2}$$

where $\hat{\mathbf{r}}_{ij} = \mathbf{r}_{ij}/r_{ij}$. We will omit the arguments when unambiguous.

Besides the operators defined in Eq. (1.2) it is convenient to introduce the projection operators

$$\begin{aligned}
\hat{P}_S &\equiv \tfrac{1}{4}(\mathbb{1} - \boldsymbol{\sigma}_1\cdot\boldsymbol{\sigma}_2),\\
\hat{P}_{T+} &\equiv \tfrac{1}{6}[3\mathbb{1} + \boldsymbol{\sigma}_1\cdot\boldsymbol{\sigma}_2 + S_{12}(\hat{\mathbf{r}})],\\
\hat{P}_{T-} &\equiv \tfrac{1}{12}[3\mathbb{1} + \boldsymbol{\sigma}_1\cdot\boldsymbol{\sigma}_2 - 2S_{12}(\hat{\mathbf{r}})].
\end{aligned} \tag{1.3}$$

These satisfy the relations $\hat{P}_i\hat{P}_j = \hat{P}_i\delta_{ij}$ and $\hat{P}_S + \hat{P}_{T+} + \hat{P}_{T-} = \mathbb{1}$.

If tensor forces are included, then a third set of operators,

$$\hat{L} \equiv (\boldsymbol{\sigma}_1\cdot\hat{\mathbf{r}})(\boldsymbol{\sigma}_2\cdot\hat{\mathbf{r}}), \quad \hat{T} \equiv \boldsymbol{\sigma}_1\cdot\boldsymbol{\sigma}_2 - (\boldsymbol{\sigma}_1\cdot\hat{\mathbf{r}})(\boldsymbol{\sigma}_2\cdot\hat{\mathbf{r}}), \tag{1.4}$$

is useful for the summation of chain diagrams [6].

The task of microscopic many-body theory is to understand properties of macroscopic systems from no other information than the properties of the underlying Hamiltonian, the particle statistics, and the macroscopic geometry of the system. For simple, state-independent interactions as appropriate for electrons or quantum fluids, the Jastrow-Feenberg ansatz [7] for the wave function

$$\Psi_0 = \prod_{\substack{i,j=1\\ i<j}}^{N} f(r_{ij})\Phi_0 \tag{1.5}$$

and its logical generalization to multiparticle correlation functions [8–12] has been extremely successful. Φ_0 is, for fermions, a Slater determinant of single-particle orbitals, and $f(r_{ij})$ is the Jastrow-Feenberg correlation function whose primary purpose is to model short-ranged correlations. The method has therefore been applied in both semianalytic calculations [7] as well as early Monte Carlo calculations [13,14] and is still being used as an importance sampling function for diffusion and Green's functions Monte Carlo computations [15,16].

One of the reasons for the success of the wave function (1.5) is that it provides a good upper bound for the ground-state energy,

$$E_0 = \frac{\langle\Psi_0|H|\Psi_0\rangle}{\langle\Psi_0|\Psi_0\rangle}. \tag{1.6}$$

In semianalytic calculations, approximations must be made in the evaluation of the energy expectation value (1.6). The hierarchy of "(Fermi-)hypernetted chain [(F)HNC]" approximations [17] is singled out since it permits an unconstrained

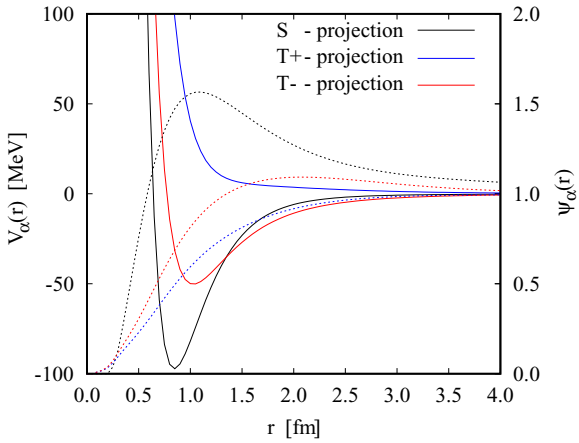

FIG. 1. The Reid interaction [1] in the $\{S, T+, T-\}$ operator form for the singlet (black line), triplet "+" (blue line), and triplet "–" (red line) projections (left scale). Also shown are the corresponding pair wave functions $\psi_\alpha(r) = \sqrt{1 + \Gamma_{\rm dd}^{(\alpha)}(r)}$, see Eq. (2.15) at $k_F = 1.0$ fm^{-1} (dashed line, same colors, right scale).

optimization of the correlation functions,

$$\frac{\delta E_0}{\delta f}(\mathbf{r}_1, \mathbf{r}_2) = 0, \tag{1.7}$$

in the sense that the Euler equations for any level of the HNC approximation has the same structure as the exact Euler equation [7]. The method corresponds, for bosons, to a self-consistent summation of all ring and ladder diagrams of perturbation theory—the so-called "parquet" diagrams [18–21]. The same is true for Fermions [22] when specific truncation orders of exchange diagrams are followed.

The Jastrow-Feenberg ansatz (1.5) is insufficient for dealing with realistic nucleon-nucleon interactions of the form (1.1). As an example, we show in Fig. 1 the Reid v_6 interaction in the three operator channels $\hat{P}_S$, $\hat{P}_{T+}$, and $\hat{P}_{T-}$. Using a correlation function that is the same in all three channels can at its best only roughly model short-ranged correlations in these different configurations.

A plausible generalization of the wave function (1.5) is the symmetrized operator product [23,24],

$$\Psi_0^{\rm SOP} = \mathcal{S}\left[\prod_{\substack{i,j=1\\ i<j}}^{N} \hat{f}(i,j)\right]\Phi_0, \tag{1.8}$$

where

$$\hat{f}(i,j) = \sum_{\alpha=1}^{n} f_\alpha(r_{ij})\,\hat{O}_\alpha(i,j), \tag{1.9}$$

and $\mathcal{S}$ stands for symmetrization. The symmetrization is necessary because the operators $\hat{O}_\alpha(i,j)$ and $\hat{O}_\beta(i,k)$ do not necessarily commute. The potential energy, for example, can be written in the form

$$\frac{\langle V\rangle}{N} = \frac{\rho}{2}\int d^3r \sum_\alpha g_\alpha(r) v_\alpha(r) \frac{1}{\nu^2}\mathcal{T}r_{12}\, O_\alpha^2(1,2), \tag{1.10}$$

where ν is the degree of degeneracy of the single-particle states, $\mathcal{T}r_{12}$ indicates the trace over spin (and, when applicable, isospin) variables of particles 1 and 2, and the components of the pair distribution function are

$$\rho^2 g_\alpha(|\mathbf{r}-\mathbf{r}'|) = \frac{\langle\Psi_0|\sum_{i<j}\delta(\mathbf{r}-\mathbf{r}_i)\delta(\mathbf{r}'-\mathbf{r}_j)\hat{O}_\alpha(i,j)|\Psi_0\rangle}{\frac{1}{\nu^2}\mathcal{T}r_{12}\,\hat{O}_\alpha^2(1,2)\langle\Psi_0|\Psi_0\rangle}. \tag{1.11}$$

The need to symmetrize the operator product causes, however, severe problems which must be dealt with properly: When the symmetrization is carried out, the components of the pair distribution operator have the form

$$g_\alpha(r) = \sum_{\beta\gamma} f_\beta(r) f_\gamma(r) F_{\beta\gamma}^{(\alpha)}(r), \tag{1.12}$$

where the $F_{\beta\gamma}^{(\alpha)}(r)$ are coupling coefficients that are functionals of the correlation functions $f_\alpha(r_{ij})$. Their analytic structure is complicated and so far no summation that comes anywhere close to the diagrammatic richness of the (F)HNC summations for state-independent correlations has been found.

The only relevant feature for our analysis is, however, that the coefficient functions $F_{\beta\gamma}^{(\alpha)}(r)$ are *not* diagonal in the operator labels α, β, and γ. In other words, the interaction in operator channel α is, in the potential energy, multiplied with correlation functions $f_\beta(r) f_\gamma(r)$ with $\beta \neq \alpha$, $\gamma \neq \alpha$.

This is *a priori* not a problem because the (observable) pair distribution functions $g_\alpha(r)$ can be thought of as the independent quantities in the variational problem, i.e., instead of Eq. (1.7) we may use

$$\frac{\delta E_0}{\delta g_\alpha}(\mathbf{r}_1, \mathbf{r}_2) = 0. \tag{1.13}$$

Then the theory can be formulated entirely in terms of observable quantities. In fact, the basic equations of the boson theory can be derived in several ways [19,20,25,26] without ever mentioning the auxiliary Jastrow correlation function $f(r)$.

However, if one adopts the original idea of Jastrow theory and uses some parameterized form of the correlation functions $f_\alpha(r)$, then a good parametrization is hard to find. A popular choice [27,28] is, for example, to derive the correlation functions $f_\alpha(r)$ from a low-order constrained variational principle (LOCV). This leads for the correlation functions to an effective Schrödinger equation of the form

$$-\frac{\hbar^2}{m}\nabla\cdot\left[g_F^{(\alpha)}(r)\nabla f_\alpha(r)\right] + [v_\alpha(r) - \lambda_\alpha] g_F^{(\alpha)}(r) f_\alpha(r) = 0. \tag{1.14}$$

Equation (1.14) is understood in the projection operator basis (1.3). The λ_α are parameters determined either by a normalization condition [27,29] or by the demand that $f_\alpha'(d) = 0$ at a healing distance d [28], and $g_F^{(\alpha)}(r) = 1 \pm \ell^2(rk_F)$ are the distribution functions of noninteracting fermions, the upper/lower sign refers to singlet/triplet states, and $\ell(x) = 3j_1(x)/x$. Modern nucleon-nucleon interactions [1–5] have rather different core sizes in the spin-singlet and the spin-triplet cases, see, for example, Fig. 1.

The above analysis shows that the commutator terms in the symmetrized operator product (1.8) mix different channels such that it is by no means clear how well the short-ranged correlations are described by simple approximations like (1.14). In fact, earlier nucleon-nucleon interaction [30,31] contained hard cores with different core sizes in different operator channels. In that case, the potential energy obtained from correlations determined by the LOCV method diverges already if only the simplest nontrivial commutator term is retained.

As an alternative to variational wave functions, Smith and Jackson [32] started from the idea of localized parquet-diagram summations and implemented the procedure for a fictive system of bosonic nucleons interacting via a v_6 interaction. It turned out that the equations derived were identical to those one would obtain in the bosonic version of the summation method of Fantoni and Rosati [23], which simply ignored the fact that the individual pair correlation operators $\hat{f}(i,j)$ do not commute. We have adopted in Ref. [33] the ideas of Smith and Jackson and generalized them to Fermi systems. In that work, we have also paid attention to different treatments of the particle-particle and the particle-hole propagator and have determined which approximations for these quantities are suggested by variational wave functions.

The problem of the potential importance of commutator diagrams does not go away in parquet summations. The fact that the work of Ref. [32] corresponds to a variational calculation where all commutators are omitted simply says that the fully symmetrized wave function (1.8) contains more than what is included in the parquet equations. The analysis (1.12) shows that these non-parquet contributions are important. On the other hand, the point of view of parquet-diagram summations promises a more straightforward procedure to deal with these effects compared to going through the development of a full variational procedure. The equivalence between classes of Feynman diagrams and classes of Jastrow-Feenberg diagrams will provide a vehicle for justifying practical procedures for their calculation. To that end, we will in the next section discuss, with a very simple example, how the physics of commutator corrections is described in terms of Goldstone diagrams and which approximations to these diagrams are suggested by a variational wave function.

Section III B will then derive the implementation of these "non-parquet" diagrams in a generalized Bethe-Goldstone equation. Numerical applications will be discussed in Sec. IV, Sec. V will provide a brief summary of our findings. The Appendix will review earlier work [34] where the symmetrization problem can be examined in a relatively simple analytic form.

II. ESSENTIALS OF PARQUET DIAGRAM SUMMATIONS AND THE OPTIMIZED HYPERNETTED CHAIN METHOD

The basic insight, which was explained quite convincingly in Ref. [19], is that the minimal satisfactory microscopic treatment of an interacting system of many identical particles requires the self-consistent summation of ring and ladder diagrams. This is in principle an exceedingly demanding task because each two body vertex is a functions of two incoming $(\mathbf{k}_i, \hbar\omega_i)$ and two outgoing sets of four quantum numbers. Energy and momentum conservation as well as isotropy lets us reduce the number of variables to 10. Hence, approximations must be made to make the theory practical which we review here.

A. Ring diagrams and the induced interaction

The ring diagrams describe low-lying excitations and long-ranged correlations. The sum of ring diagrams diverges when the system is unstable against low-lying excitations such as density- or spin-density fluctuations. Therefore, their inclusion is important to have the correct nonanalytic density dependence of the equation of state of a self-bound system.

These are derived from a random-phase approximation (RPA) equation for the response function,

$$\hat{\chi}(q,\omega) = \frac{\chi_0(q,\omega)}{1-\hat{V}_{\mathrm{p-h}}(q)\chi_0(q,\omega)}$$
$$S(q) = -\int_0^\infty \frac{d\hbar\omega}{\pi}\mathrm{Im}\,\chi(q,\omega), \tag{2.1}$$

in terms of a local "particle-hole" interaction $\hat{V}_{\mathrm{p-h}}(q)$. In the case of state-dependent interactions, $\hat{V}_{\mathrm{p-h}}(q)$ is most conveniently represented as a linear combination of local functions $\tilde{V}^{(\alpha)}_{\mathrm{p-h}}(q)$ and the operators (1.4). As usual we define the dimensionless Fourier transform by including a density factor ρ, i.e.,

$$\tilde{f}(k) = \rho\int d^3r f(r)e^{i\mathbf{k}\cdot\mathbf{r}} = \rho\int d^3r f(r) j_0(kr). \tag{2.2}$$

For the tensor forces, we will also need the j_2 Fourier transform,

$$\tilde{f}(k)S_{12}(\hat{\mathbf{k}}) = \rho\int d^3r f(r)e^{i\mathbf{k}\cdot\mathbf{r}}S_{12}(\hat{\mathbf{r}})$$
$$= -\rho\int d^3r f(r) j_2(kr)S_{12}(\hat{\mathbf{k}}). \tag{2.3}$$

The second important relationship is the Bethe-Goldstone equation which describes short-ranged correlations caused by the strong, short-ranged repulsion of the nuclear interaction. We shall discuss this in detail below. Summing the parquet diagrams one supplements, among others, the bare interaction $\hat{v}(\mathbf{r})$ in the Bethe-Goldstone equation by an induced interaction $\hat{w}_I(\mathbf{r})$ being defined as the set of particle-hole reducible diagrams. Assuming a particle-hole interaction $\hat{V}_{\mathrm{p-h}}(\mathbf{q})$ of the operator of the form (1.2), the sum of these diagrams is *a priori* an energy-dependent quantity,

$$\hat{w}_I(\mathbf{q},\omega) = \frac{\hat{V}^2_{\mathrm{p-h}}(\mathbf{q})\chi_0(q,\omega)}{1-\hat{V}_{\mathrm{p-h}}(\mathbf{q})\chi_0(q,\omega)}. \tag{2.4}$$

The energy-dependent-induced interaction is then approximated [19,20] by an energy-independent effective interaction $\hat{w}(q)$ as follows: Calculate the static structure function

$$S(\mathbf{q}) = -\int_0^\infty \frac{d\hbar\omega}{\pi}\,\mathrm{Im}\frac{\chi_0(q,\omega)}{1-\chi_0(q,\omega)\hat{V}_{\mathrm{p-h}}(\mathbf{q})}$$
$$= -\int_0^\infty \frac{d\hbar\omega}{\pi}\,\mathrm{Im}\big[\chi_0(q,\omega)+\chi_0^2(q,\omega)\hat{w}(\mathbf{q},\omega)\big]. \tag{2.5}$$

Now define an *energy-independent interaction* $\hat{w}_I(q, \bar{\omega}(q))$ by demanding that it gives the same static structure function,

$$S(q) \equiv -\int_0^\infty \frac{d\hbar\omega}{\pi} \mathrm{Im}\big[\chi_0(q,\omega) + \chi_0^2(q,\omega)\hat{w}(q,\bar{\omega}(q))\big]. \tag{2.6}$$

This energy-independent interaction $\hat{w}(\mathbf{q}) \equiv \hat{w}(\mathbf{q}, \bar{\omega}(q))$ defines the induced interaction $\hat{w}_I(q) \equiv \hat{w}(q) - \hat{V}_{\mathrm{p-h}}(q)$ which is then taken as a correction to the interaction in the Bethe-Goldstone equation. For state-dependent interactions it is again understood that $\hat{w}_I(\mathbf{q}, \omega)$ is a linear combination of local functions and operators of any of the forms (1.2), (1.3), or (1.4).

B. Localized Bethe-Goldstone equation

We review here briefly the connection between the conventional Bethe-Goldstone equation and the variational approach. We begin with the Bethe-Goldstone equation as formulated in Eqs. (2.1) and (2.2) of Ref. [35]. As a convention, we will label occupied ("hole") states by $\mathbf{h}, \mathbf{h}', \mathbf{h}_i$ and unoccupied ("particle") states by $\mathbf{p}, \mathbf{p}', \mathbf{p}_i$; whereas $\mathbf{k}, \mathbf{q}$ have no restriction. We also suppress spin variables. The pair wave function $\psi(k)$ in a coordinate frame centered at the origin of the Fermi sea is given by the integral equation

$$\langle \mathbf{k},\mathbf{k}'|\psi|\mathbf{h},\mathbf{h}'\rangle = \langle \mathbf{k},\mathbf{k}'|\mathbf{h},\mathbf{h}'\rangle - \bar{n}(k)\bar{n}(k')\frac{\langle \mathbf{k},\mathbf{k}'|\hat{V}\psi|\mathbf{h},\mathbf{h}'\rangle}{t(k)+t(k')-t(h)-t(h')}, \tag{2.7}$$

where $n(k) = \theta(k_F - k)$ is the Fermi distribution, $\bar{n}(k) = 1 - n(k)$ and, in the simplest case, $t(k) = \hbar^2k^2/2m$. In the conventional Bethe-Goldstone equation, $\hat{V}$ was meant to be the bare interaction operator $\hat{v}$. In FHNC-EL or parquet-theory, $\hat{v}$ is supplemented by the induced interaction $\hat{w}_I$ defined in Eq. (2.6). We can also have "non-parquet" diagrams—in (F)HNC-EL these are due to "elementary diagrams" and multiparticle correlations, while in the language of perturbation theory these are particle-particle and particle-hole irreducible vertices. Thus, in general, we may assume

$$\hat{V}(i,j) = \hat{v}(i,j) + \hat{w}_I(i,j) + \hat{V}_I(i,j), \tag{2.8}$$

where $\hat{V}_I(i,j)$ is the set of irreducible diagrams. All three sets are assumed to have the operator structure (1.1).

The pair wave function ψ is still a function of three momenta. On the other hand, the variational wave function (1.8) contains only functions that depend on the distance between two particles. To make a connection between perturbation theory and the variational wave function, we must therefore approximate the pair wave function by a quantity that depends only on the relative coordinate (or momentum), i.e., it has the feature

$$\langle \mathbf{k},\mathbf{k}'|\psi|\mathbf{h},\mathbf{h}'\rangle = \frac{1}{N}\tilde{\psi}(q).$$

For local interactions, we then have also

$$\langle \mathbf{k},\mathbf{k}'|v\psi|\mathbf{h},\mathbf{h}'\rangle = \frac{1}{N}[v(r)\psi(r)]^{\mathcal{F}}(q),$$

where $\mathcal{F}$ stands for the Fourier transform (2.2) or (2.3). To have such a solution, the energy denominator coefficient must be approximated by a function of momentum transfer q. One option is to write Eq. (2.7) as

$$[t(k)+t(k')-t(h)-t(h')][\langle \mathbf{k},\mathbf{k}'|\psi|\mathbf{h},\mathbf{h}'\rangle - \langle \mathbf{k},\mathbf{k}'|\mathbf{h},\mathbf{h}'\rangle] = -\bar{n}(k)\bar{n}(k')\langle \mathbf{k},\mathbf{k}'|v\psi|\mathbf{h},\mathbf{h}'\rangle, \tag{2.9}$$

and then approximate the particle-hole energy differences by their Fermi-sea average,

$$t(|\mathbf{h}+\mathbf{q}|) - t(h) \approx \frac{\sum_{\mathbf{h}} \bar{n}(|\mathbf{h}+\mathbf{q}|)n(h)t(|\mathbf{h}+\mathbf{q}|) - t(h)}{\sum_{\mathbf{h}} \bar{n}(|\mathbf{h}+\mathbf{q}|)n(h)} = \frac{t(q)}{S_F(q)} \equiv t_F(q). \tag{2.10}$$

This leads to

$$\left[-\frac{\hbar^2}{m}\nabla^2 + v(r)\right]\psi(r) = -\frac{\rho}{\nu}\int d^3r'\ell^2(|\mathbf{r}-\mathbf{r}'|k_F)v(r')\psi(r'), \tag{2.11}$$

see Ref. [33] for a different but equivalent way to write this equation. Equation (2.11) is very similar to the Bethe-Goldstone equation for a pair of particles whose center-of-mass momentum is zero. In that case, one obtains [35,36]

$$\left[-\frac{\hbar^2}{m}\nabla^2 + v(r)\right]\psi(r) = -\frac{\rho}{\nu}\int d^3r'\ell(|\mathbf{r}-\mathbf{r}'|k_F)v(r')\psi(r'). \tag{2.12}$$

The G matrix is, in the local approximation, given by

$$\hat{G}(\mathbf{q}) = \hat{V}(\mathbf{q}) - \int \frac{d^3q'}{(2\pi)^3}\hat{V}(|\mathbf{q}-\mathbf{q}'|)\frac{\hat{G}(\mathbf{q}')}{2t_F(q')}. \tag{2.13}$$

The convolution product is best written in coordinate space,

$$\hat{G}(\mathbf{r}) = \hat{V}(\mathbf{r}) - \hat{V}(\mathbf{r})\left[\frac{\hat{G}(\mathbf{q})}{2t_F(q)}\right]^{\mathcal{F}}(\mathbf{r}). \tag{2.14}$$

We have above not explicitly spelled out the operator dependence which is implied. The equations are the same for state-dependent interactions, they separate in the projector representation $\{\hat{P}_S, \hat{P}_{T+}, \hat{P}_{T-}\}$.

We stress here that the local "particle-hole" interaction $\hat{V}_{\mathrm{p-h}}(\mathbf{q})$ entering the summation of ring diagrams must *not* be identified with some local approximation of the G matrix. This is seen most easily in a self-bound system like nuclear matter by the argument that the Fermi-sea average of the G matrix should basically be the interaction correction to the binding energy which is negative. On the other hand, the matrix element of the central component of $\hat{V}_{\mathrm{p-h}}(\mathbf{q})$ at the Fermi surface is the interaction correction to the incompressibility which is positive [37]. The problem is not as significant for repulsive systems like neutron matter studied here or for electrons [38], we see, on the other hand, no reason to make such unnecessary approximations.

The FHNC-EL equations lead to a slightly different form [39], but note that FHNC sums more than just the

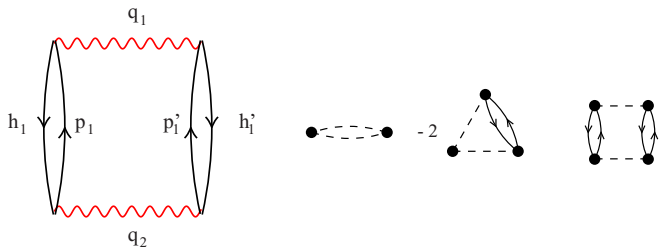

FIG. 2. The left diagram is the second-order Goldstone diagram, the wiggly line represents an interaction. The three diagrams on the right-hand side are the corresponding JF diagrams, the usual diagrammatic conventions [42] apply: The dashed line represent correlation factors $h(r_{ij})$ and the oriented solid ones represent exchange lines $\ell(r_{ij}k_F)$.

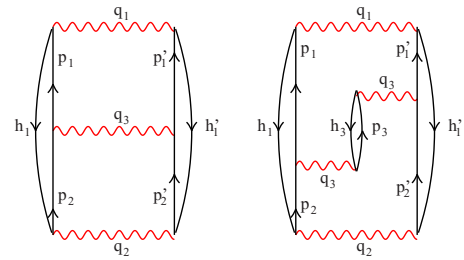

FIG. 3. The simplest ladder diagrams. The left diagram is the ordinary three-rung ladder, the right one contains an induced interaction.

particle-particle ladders. We found, however, in our numerical applications that the numerical solutions are very close. We shall, therefore, not elaborate on this issue any further. Diagrammatically we can identify the pair wave function $\psi(r)$ with the direct correlation function $\Gamma_{\rm dd}(r)$,

$$\psi(r) = \sqrt{1 + \Gamma_{\rm dd}(r)}. \tag{2.15}$$

III. BEYOND PARQUET: INCLUDING "TWISTED CHAIN" DIAGRAMS

A. Low order analysis

We now turn to the main issue of this work, which is the diagrammatic content and the treatment of the commutator terms introduced by the need to symmetrize the operator product (1.8). For this purpose, we utilize the correspondence between diagrams of the cluster expansions for Jastrow-Feenberg wave functions and specific approximations to Goldstone diagrams. Such a correspondence has been observed a long time ago [40,41]. In a very vague language, Jastrow-Feenberg diagrams and Goldstone diagrams can be identified by absorbing the energy denominator in the interaction which then defines a dimensionless function $h(r_{ij})$. What remains is only the momentum flux and the Pauli operators.

The rules on how to translate a Goldstone diagrams into a Jastrow-Feenberg diagram are then easily verified:

(i) Reinterpret each interaction line by a correlation function $h(r_{ij}) = f^2(r_{ij}) - 1$.
(ii) Omit all energy denominators.
(iii) Each hole line turns into an exchange line $\ell(r_{ij}k_F)$, where $\ell(x) = \frac{3}{x} j_1(x)$.
(iv) Each particle line turns into $\delta(r_{ij}) - \ell(r_{ij}k_F)$.

There cannot be an exact one-to-one correspondence because the wave function (1.5) or (1.8) is defined for *any* correlation function, whereas the sum of all Goldstone diagrams converges toward the exact ground state. To make the connection complete one must also include the optimization of the correlations.

To see how this works, we consider the simple second-order perturbation theory. To simplify the notation, we do this for central interactions only. The left figure in Fig. 2 is the second-order Goldstone diagram, and the right figure is what would result from the above operations. Note that the first of the JF diagrams does not appear in cluster expansions of the Jastrow-Feenberg wave function.

Let us next see how the localization procedure (2.6) of parquet theory works in the case of a simple ladder diagram. Figure 3 shows the third-order ladder diagram in which the middle rung in the left diagram is replaced by an induced interaction in the right diagram.

The exact form of the left diagram is, for local translationally invariant interactions,

$$\frac{1}{N^3} \sum_{q_i h_1 h_1'} \tilde{v}(q_1) \frac{\bar{n}(\mathbf{h}_1 + \mathbf{q}_1)\bar{n}(\mathbf{h}_1' - \mathbf{q}_1)}{e_{\mathbf{h}_1+\mathbf{q}_1} + e_{\mathbf{h}_1'-\mathbf{q}_1} - e_{h_1} - e_{h_1'}} \times \tilde{v}(\mathbf{q}_1 - \mathbf{q}_2) \frac{\bar{n}(\mathbf{h}_1 + \mathbf{q}_2)\bar{n}(\mathbf{h}_1' - \mathbf{q}_2')}{e_{\mathbf{h}_1+\mathbf{q}_2} + e_{\mathbf{h}_1'-\mathbf{q}_2} - e_{h_1} - e_{h_1'}} \tilde{v}(q_2). \tag{3.1}$$

We can write the right diagram in Fig. 3 in a similar way,

$$\frac{1}{N^3} \sum_{q_i h_1 h_1'} \tilde{v}(q_1) \frac{\bar{n}(\mathbf{h}_1 + \mathbf{q}_1)\bar{n}(\mathbf{h}_1' - \mathbf{q}_1)}{e_{\mathbf{h}_1+\mathbf{q}_1} + e_{\mathbf{h}_1'-\mathbf{q}_1} - e_{h_1} - e_{h_1'}} \times \tilde{w}\big(\mathbf{q}_1 - \mathbf{q}_2, e_{\mathbf{h}_1+\mathbf{q}_1} + e_{\mathbf{h}_1'-\mathbf{q}_2} - e_{h_1} - e_{h_1'}\big) \times \frac{\bar{n}(\mathbf{h}_1 + \mathbf{q}_2)\bar{n}(\mathbf{h}_1' - \mathbf{q}_2')}{e_{\mathbf{h}_1+\mathbf{q}_2} + e_{\mathbf{h}_1'-\mathbf{q}_2} - e_{h_1} - e_{h_1'}} \tilde{v}(q_2), \tag{3.2}$$

with an energy-dependent interaction,

$$\tilde{w}(q, \hbar\omega) = -\tilde{v}^2(q) \frac{1}{N} \sum_h \frac{1}{e_{\mathbf{h}+\mathbf{q}} - e_h + \hbar\omega}. \tag{3.3}$$

The localization procedure of parquet theory replaces the energy-dependent-induced interaction $\tilde{w}(q, \hbar\omega)$ by an energy-independent interaction which is constructed from $\tilde{w}(q, \hbar\omega)$ by evaluating this quantity at an averaged frequency $\bar{\omega}(q)$, i.e.,

$$\tilde{w}(q) = \tilde{w}(q, \hbar\bar{\omega}(q)), \tag{3.4}$$

see Eq. (2.6). Once $\tilde{w}(q, \hbar\omega)$ has been replaced by $\tilde{w}(q) = \tilde{w}(q, \hbar\bar{\omega}(q))$, the combination $\tilde{v}(q) + \tilde{w}(q)$ can be used as an effective interaction in the Bethe-Goldstone equation; this is exactly the connection between the parquet-diagram and the (F)HNC-EL view of ground-state correlations.

In the next order, shown in Fig. 4, we first see the possibility of "twisting" chain diagrams.

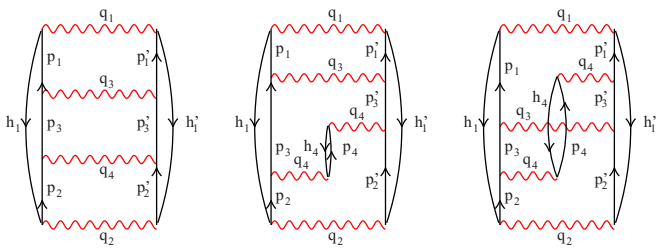

FIG. 4. Fourth-order ladder diagrams, including a "twisted chain" diagram. The left diagram is the four-body ladder, in the middle diagram one of the interactions is replaced by an induced interaction, and the right one the twisted version.

The left and the middle diagrams can again be combined by introducing the energy-dependent-induced interaction $\tilde{w}(q, \hbar\omega)$ which is then, in the local approximation, replaced by $\tilde{w}(q)$ as in Eq. (3.4).

The third diagram, although it has the same components, is by its very definition not a parquet diagrams, and cannot be represented in terms of the energy-dependent interaction $\tilde{w}(q, \hbar\omega)$. Apply now the rules, discussed in connection with Fig. 2, for how to identify Goldstone and Jastrow-Feenberg diagrams and re-interpret the second and third diagram shown in Fig. 4 as Jastrow-Feenberg diagrams. We then find that these two diagrams have indeed the same value, i.e., the Jastrow-Feenberg wave function suggests to approximate these two terms by the same quantity. We can therefore conclude that, *if* we want to approximate the cross-going portion in the third diagram by a static interaction, this should be the same as the induced interaction $\tilde{w}(q, \omega)$. Moreover, the equivalence of Jastrow-Feenberg theory and the local parquet theory shows that the FHNC-EL approximation contains *both* terms.

The above analysis is valid only for state-independent interactions or correlations or, in other words, for the configuration-space components of this diagram. There is no reason that the same argument should work for the spin/isospin components. Assume therefore now that interactions are state dependent. For the present purpose, it is best to represent them in the $\{\mathbb{1}, \hat{L}, \hat{T}\}$ basis, then the operators on the interactions with momentum transfer q_4 must be the same, say, $\hat{O}_\alpha$ and the operator associated with the interaction with momentum transfer q_4 be $\hat{O}_\beta$. We were above led to the conclusion that variational wave functions suggest the approximation that the coordinate or momentum dependence of the subdiagrams with momentum transfer q_4 are the same, but the operator dependence has to be included more carefully. The second diagram in Fig. 4 has then the operator structure

$$\mathcal{T}r_4[\hat{O}_\alpha(14)\hat{O}_\alpha(42)\hat{O}_\beta(12)],$$

whereas the third diagram has the operator order

$$\mathcal{T}r_4[\hat{O}_\alpha(14)\hat{O}_\beta(12)\hat{O}_\alpha(42)],$$

i.e., the combination of these two operators is exactly the symmetrized product.

The way to correct the parquet equations [32] or the version of the (F)HNC equations that ignores all commutators [23] is therefore to add the commutator of these two terms.

$$\tfrac{1}{2}\mathcal{T}r_4[\hat{O}_\alpha(14)[\hat{O}_\beta(12), \hat{O}_\alpha(42)]].$$

B. Twisted chains corrections to the Bethe Goldstone equation

We now turn to including the "twisted chain" diagrams in the localized Bethe-Goldstone equation.

We have two diagrammatic elements: The bare interaction $\hat{v}(\mathbf{q})$ which is completely irreducible and the induced interaction $\hat{w}_I(\mathbf{q})$, which is particle-hole reducible and comes from the FHNC-EL equations or is constructed by means of the "average energy" approximation (3.4). The bare interaction comes always in combination with the induced interaction, we will depict the sum of these two as a magenta wiggled line. For the following calculations, we assume that both the bare interaction $\hat{v}(i, j)$ and the induced interaction $\hat{w}_I(i, j)$ are given in the operator basis $\{\mathbb{1}, \hat{L}, \hat{T}\}$. In that basis, it is sufficient to consider chains of two elements as shown in Fig. 4, the longer chains left and right of the particle-hole bubble $\{p_4, h_4\}$ can be summed into one term.

The "cross-going" diagrams, i.e., those of the topology of the third diagram shown in Fig. 4 must all be particle-hole reducible, we will depict these as blue wiggled lines. As we have shown above, the Jastrow-Feenberg wave function suggests that configuration space of the second and the third diagram in Fig. 4 are the same and all we need to do is to include the commutators.

Let us assume that the operator connected with the interaction line $\hat{v} + \hat{w}_I$ in Fig. 4 is $\hat{O}_v(i, j)$. The operator connected with the induced interaction is $\hat{O}_w(i, j)$. These operators are either $\hat{L}(i, j) = \sigma_\alpha(i)t^{(L)}_{\alpha\beta}(\hat{\mathbf{r}})\sigma_\beta(j), t^{(L)}_{\alpha\beta} = \hat{r}_\alpha\hat{r}_\beta$ or $\hat{T}(i, j) = \sigma_\alpha(i)t^{(T)}_{\alpha\beta}(\hat{\mathbf{r}})\sigma_\beta(j), t^{(T)}_{\alpha\beta} = \hat{r}_\alpha\hat{r}_\beta - \delta_{\alpha\beta}$. We will also need the same set of operators in momentum space, the unit vector $\hat{\mathbf{r}}$ is then replaced by $\hat{\mathbf{q}}$. We label the *external* points with a, b and the *internal* points with numbers. The *correction* to the unsymmetrized operator product is then given by the commutator

$$\tfrac{1}{2}\mathcal{T}r_1[\hat{O}_w(a, 1)[\hat{O}_v(a, b), \hat{O}_w(1, b)]], \tag{3.5}$$

where the $\hat{O}_w$ are the spin-operators associated with the induced interaction $\hat{w}_I$ and $\hat{O}_v$ are those associated with $\hat{v} + \hat{w}_I$. The commutator with the central operator is evidently zero. In what follows, we will also need the relationships

$$\hat{L}^2 = \hat{P}_S + \hat{P}_{T+} + \hat{P}_{T-} = \mathbb{1}, \tag{3.6a}$$

$$\hat{T}^2 = 4\hat{P}_S + 4\hat{P}_{T-} = 2\mathbb{1} - 2\hat{L}, \tag{3.6b}$$

$$\hat{L}\hat{T} = 2\hat{P}_S - 2\hat{P}_{T-} = -\hat{T}. \tag{3.6c}$$

For both the longitudinal and the transverse operators, we have $\sum_\beta t_{\alpha\beta}t_{\beta\mu} = t_{\alpha\mu}$, we get therefore for (3.5)

$$\begin{aligned}&\mathcal{T}r_1\left[\sigma_\alpha(a)t^{(w)}_{\alpha\beta}\sigma_\beta(1)\sigma_\gamma(a)t^{(v)}_{\gamma\delta}\sigma_\delta(b)\sigma_\lambda(1)t^{(w)}_{\lambda\mu}\sigma_\mu(b)\right]\\ &\quad - \nu O_v(a, b)O_w(a, b)\\ &= -2\nu O_v(a, b)O_w(a, b) + 2\nu t^{(w)}_{\alpha\beta}t^{(v)}_{\alpha\beta}.\end{aligned}$$

We must now distinguish three cases:

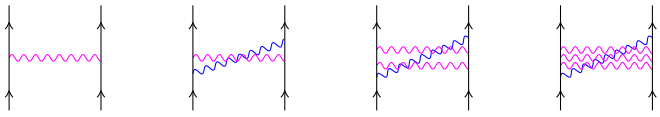

FIG. 5. Examples where the reducible induced interaction crosses more than one rung. The magenta line represents the sum $\hat{v} + \hat{w}_I$. The rungs can all be summed to the G matrix.

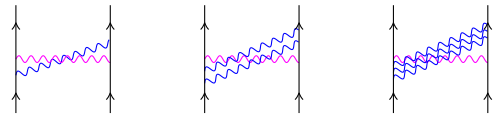

FIG. 6. The summation of more than one cross-going lines.

(i) Both $\hat{O}_v(a,b) = \hat{O}_w(a,b) = \hat{L}(a,b)$. Use Eq. (3.6a):

$$-2v\hat{L}^2(a,b) + 2vt^{(L)}_{\alpha\beta}t^{(L)}_{\alpha\beta} = 0. \tag{3.7}$$

(ii) $\hat{O}_v(a,b) = \hat{L}(a,b)$ and $\hat{O}_w(a,b) = \hat{T}(a,b)$. Use Eq. (3.6c):

$$-2v\hat{L}(a,b)\hat{T}(a,b) + 2vt^{(L)}_{\alpha\beta}t^{(T)}_{\alpha\beta} = 2v\hat{T}(1,2). \tag{3.8}$$

(iii) Both $\hat{O}_v(a,b) = \hat{O}_w(a,b) = \hat{T}(a,b)$. Use Eq. (3.6b):

$$-2v\hat{T}(a,b)^2 + 2vt^{(T)}_{\alpha\beta}t^{(T)}_{\alpha\beta} = 4v\hat{L}(a,b). \tag{3.9}$$

So far we have only considered the simplest process. Next, consider the series shown in Fig. 5. The summation of these diagrams is necessary to deal with short-ranged correlations.

The diagram with n rungs and one crossing has the spin-operator structure

$$\mathcal{T}r_1\big[\hat{O}_w(a,1)\hat{O}_{v_1}(a,b)\ldots,\hat{O}_{v_n}(a,b)\hat{O}_w(b,1) - \hat{O}_{v_1}(a,b)\ldots,\hat{O}_{v_n}(a,b)\hat{O}_w(a,1)\hat{O}_w(b,1)\big]$$

where the O_{v_i} are the spin-operators connected to the n rungs. These are *a priori* from the set $\{\mathbb{1},\hat{L},\hat{T}\}$. We rewrite the product $\hat{O}_{v_1}(a,b),\ldots,\hat{O}_{v_n}(a,b)$ in terms of the projection operators (1.3). All of these operators have, in coordinate space, the same spatial argument $\hat{\mathbf{r}}$. They are therefore idempotent and, hence, the product $\hat{O}_{v_1}(a,b),\ldots,\hat{O}_{v_n}(a,b)$ can be rewritten as a linear combination of the projection operators (1.3) which, at the end, is transformed to a linear combination of the set $\{\mathbb{1},\hat{L},\hat{T}\}$. The conclusion is that sum of all magenta lines in Fig. 5 can be represented by the G matrix.

Similarly, we can calculate the set of diagrams shown in Fig. 6. Note that we can here, according to the above, interpret the magenta wavy line as a component of the G matrix. Then the operator form of a diagram with n crossing rungs in Fig. 6 is

$$\mathcal{T}r_{1\ldots n}\big[\hat{O}_{w_1}(a,1)\cdots\hat{O}_{w_n}(a,n)\hat{O}_v(a,b)\hat{O}_{w_1}(1,b)\cdots\hat{O}_{w_n}(n,b) - \hat{O}_v(a,b)\hat{O}_{w_1}(a,1)\hat{O}_{w_1}(1,b)\cdots\hat{O}_{w_n}(a,n)\hat{O}_{w_n}(n,b)\big]. \tag{3.10}$$

To evaluate this expression, we use

$$\hat{O}_v(a,b) = \frac{1}{v}\mathcal{T}r_{n+1}[\hat{O}_v(a,n+1)\hat{O}_v(n+1,b)]. \tag{3.11}$$

Therefore, Eq. (3.10) can be rewritten in the form

$$\begin{aligned}
&\frac{1}{v}\mathcal{T}r_{1\ldots n+1}\big[\hat{O}_v(n+1,b)\hat{O}_{w_1}(a,1)\hat{O}_{w_1}(1,b)\ldots\hat{O}_{w_n}(a,n)\hat{O}_{w_n}(1,n)\hat{O}_v(a,n+1)\big]\\
&\quad-\mathcal{T}r_{1\ldots n}\big[\hat{O}_v(a,b)\hat{O}_{w_1}(a,1)\hat{O}_{w_1}(1,b)\ldots\hat{O}_{w_n}(a,n)\hat{O}_{w_n}(n,b)\big]\\
&=\frac{v^n}{v}\mathcal{T}r_{n+1}\big[\hat{O}_v(n+1,b)\hat{O}_{w_1}(a,b)\ldots\hat{O}_{w_n}(a,b)\hat{O}_v(a,n+1)\big]\\
&\quad-v^n\big[\hat{O}_v(a,b)\hat{O}_{w_1}(a,b)\ldots O_{w_n}(a,b)\big].
\end{aligned} \tag{3.12}$$

We can now use the same argument as above to show that the product $\hat{O}_{w_1}(a,b)\cdots O_{w_n}(a,b)$ can be written as a linear combination of the operator set $\{\mathbb{1},\hat{L},\hat{T}\}$. Summing over all the blue lines in Fig. 6 gives just another Bethe-Goldstone equation in which the $\hat{v}+\hat{w}$ is replaced by the $\hat{w}$. This defines a modified G matrix, say, $\hat{G}^{(w)}$, where all the rungs are just induced interactions.

Summarizing, the Bethe-Goldstone Eq. (2.13) with the effective interaction (2.8) is supplemented by a second equation that sums the rungs containing only induced interaction lines

$$\hat{G}^{(w)}(q) = \hat{w}_I(q) - \int\frac{d^3q'}{(2\pi)^3}\hat{w}_I(\mathbf{q}-\mathbf{q}')\frac{\hat{G}^{(w)}(q')}{2t_F(q')}. \tag{3.13}$$

Along with the calculation of the G matrix we obtain the pair wave function $\tilde{\psi}(q)$, Eq. (2.11) and an analogous quantity $\tilde{\psi}^{(w)}(q)$ corresponding to $\tilde{G}^{(w)}(q)$.

The above integral Eqs. (2.13) and (3.13) sum the two types of ladder diagrams. The purpose of the summations shown in Figs. 5 and 6 was to demonstrate that we can replace the sum of all magenta wavy line by $\hat{G}(\mathbf{r})$ and the sum of all blue lines by $\hat{G}^{(w)}(\mathbf{r})$.

C. The irreducible part of the interactions

Equations (2.13) and (3.13) are solved in the $\{P_S,P_{T+},P_{T-}\}$ basis, we obtain therefore the operators in the representation

$$\begin{aligned}
\hat{G}(\mathbf{r}) &= G_S(r)\hat{P}_S + G_{T+}(r)\hat{P}_{T+} + G_{T-}(r)\hat{P}_{T-}\\
&= \sum_\alpha G_\alpha(r)\hat{P}_\alpha,
\end{aligned} \tag{3.14}$$

and the same form for $\hat{G}^{(w)}(\mathbf{r})$. To calculate the correction $\hat{V}_I(\mathbf{q})$ we now go back to the analysis of Fig. 4. We first rewrite both quantities in the basis $\{\mathbb{1}, \hat{L}, \hat{T}\}$. We can then use the coupling coefficients derived in Eqs. (3.7)–(3.9). We can then write

$$\hat{V}_I(\mathbf{q}) = -\sum_{\alpha,\beta}\int \frac{d^3q'}{2(2\pi)^3\rho}\tilde{G}_\alpha(|\mathbf{q}-\mathbf{q}'|)\frac{\tilde{G}^{(w)}_\beta(q')}{2t_F(q')} \times \mathcal{T}r_1[\hat{O}_\beta(a,1)[\hat{O}_\alpha(a,b),\hat{O}_\beta(1,b)]], \quad (3.15)$$

where it is implied that the operators $O_\alpha(a,b)$ are from the set $\{\mathbb{1}, \hat{L}, \hat{T}\}$. Of course, the commutator with the central operator $\mathbb{1}$ is zero. Using Eqs. (3.7)–(3.9) gives $\hat{V}_I(\mathbf{r})$ in the same basis, we must therefore transform back to $\{P_S, P_{T+}, P_{T-}\}$ basis. From Eqs. (3.14) we finally obtain $\hat{G}(\mathbf{r})$ and $\hat{G}^{(w)}(\mathbf{r})$ in the projector basis $\{P_S, P_{T+}, P_{T-}\}$.

$$V_I^{(S)}(r) = -\tfrac{1}{8}G_S(r)\big[-3\psi_S^{(w)}(r)+2\psi_{T+}^{(w)}(r)+\psi_{T-}^{(w)}(r)\big] - \tfrac{1}{4}G_{T+}(r)\big[\psi_S^{(w)}(r)-\psi_{T-}^{(w)}(r)\big] - \tfrac{1}{8}G_{T-}(r)\big[\psi_S^{(w)}(r)-2\psi_{T+}^{(w)}(r)+\psi_{T-}^{(w)}(r)\big], \quad (3.16a)$$

$$V_I^{(T+)}(r) = -\tfrac{1}{8}G_S(r)\big[\psi_S^{(w)}(r)-\psi_{T-}^{(w)}(r)\big] + \tfrac{1}{8}G_{T-}(r)\big[\psi_S^{(w)}(r)-\psi_{T-}^{(w)}(r)\big], \quad (3.16b)$$

$$V_I^{(T-)}(r) = -\tfrac{1}{8}G_S(r)\big[\psi_s^{(w)}-2\psi_{T+}^{(w)}(r)+\psi_{T-}^{(w)}(r)\big] + \tfrac{1}{4}G_{T+}(r)\big[\psi_S^{(w)}(r)-\psi_{T-}^{(w)}(r)\big] - \tfrac{1}{8}G_{T-}(r)\big[\psi_S^{(w)}(r)+2\psi_{T+}^{(w)}(r)-3\psi_{T-}^{(w)}(r)\big]. \quad (3.16c)$$

Equations (3.16a)–(3.16c) show exactly the conclusion drawn from the analysis of the symmetrized operator product wave function: The process described by diagrams of the kind discussed in Figs. 5 and 6 mix interaction components in different channels. Self-consistency is obtained by inserting the irreducuble terms $V_I^{(\alpha)}(r)$ in the effective interaction (2.8) and repeating the process to convergence.

IV. RESULTS

We have chosen in this work to study neutron matter for a number of reasons. Neutron matter is, apart from the complications arising from the state dependence of the interactions, one of the simplest systems of interest. As opposed to liquid ^{3}He and nuclear matter, neutron matter is not self-bound. A self-bound Fermi system has necessarily at least two spinodal points below saturation density. An immediate consequence of that is that the equation of state is a nonanalytic function of the density. Therefore, any expansion of the equation of state in powers of the density cannot converge up to equilibrium density. This complication does not exist in neutron matter and we can focus on the problem at hand, which is the treatment of operator-dependent correlations.

A consequence of the simplicity of neutron natter is, of course, that relatively primitive approximations can lead, for some quantities, to reasonable results. This is particularly true for the equation of state because the error in the energy is of second order in the error in the wave function. We must therefore look at quantities that depend sensitively on the quality of the treatment of the many-body problem. These are mostly effective interactions which are the essential input for studying pairing properties (see Refs. [43–45] for review articles) and the density response of neutron matter which have been discussed for decades [46–48].

We have carried out calculations for the Reid v_6 interaction [3] and the v_6 version of the Argonne interaction [4]. The results are very similar and no insight is gained from comparing these two interactions. We therefore report results for the Reid potential only in the density regime $0.25\ \text{fm}^{-1} \leqslant k_F \leqslant 1.8\ \text{fm}^{-1}$. The calculations to be presented here refer to what we called in Ref. [33] the "parquet//1" version. The approximation goes beyond Jastrow-Feenberg in the sense that propagator corrections are included in both the particle-particle and the particle-hole channels. The notion "//1" refers to the inclusion of first-order exchange diagrams. These are necessary to have a reasonably good agreement with the long-wavelength limit $\hat{V}_{\text{p-h}}(0+)$ and the Fermi-Liquid parameters from hydrodynamic derivatives, see Refs. [39] and [33] for a discussion. Our calculations to be presented here go beyond the work of Ref. [33] by including diagrams that would correspond to non-parquet diagrams in the language of perturbation theory, or to commutator diagrams in the language of the variational Jastrow-Feenberg method.

A. Interaction corrections

One expects the most pronounced consequence of including "twisted chain" diagrams in coordinate space at short and intermediate distances. Figure 7 shows, at $k_F = 1.0\ \text{fm}^{-1}$, the G matrix in the local approximation (2.13), the induced interaction $w_I(r)$, and the "twisted chain" correction $V_I(r)$. We also show the individual components that were spelled out in Eqs. (3.16a)–(3.16c). For example $[G^{(S)}\psi^{(w)}](r)$ shows the contribution from the first line in Eq. (3.16a), $[G^{(T+)}\psi^{(w)}](r)$ the one from the second line and $[G^{(T-)}\psi^{(w)}](r)$ the last term. The corresponding information for the $T+$ and the $T-$ projections is shown in the second and third figure, note that $[G^{(T+)}\psi^{(w)}](r)$ has no component in the $T+$ channel.

In all three channels we observe the same features: The induced interaction $w_I(r)$ is rather smooth and relatively long-ranged, whereas the non-parquet diagram contributions are localized at short and intermediate distances; this is similar to the contribution from "elementary diagram" and three-body correlations in quantum fluids. The reason for this is simply the fact that $V_I(r)$ falls off roughly like the product of the interaction and $\psi^{(w)}(r)$.

In the singlet channel, the non-parquet corrections practically double the repulsive induced interaction around the potential minimum, it appears that this is a direct consequence of the large hard core of the triplet channel potentials that is mixed into the singlet channel. What is more important is that $V_I(r)$ is in all three channels comparable to the induced interaction. On the other hand, the effect is practically irrelevant in the triplet channels because all many-body corrections are overwhelmed by the larger core size of the bare interaction.

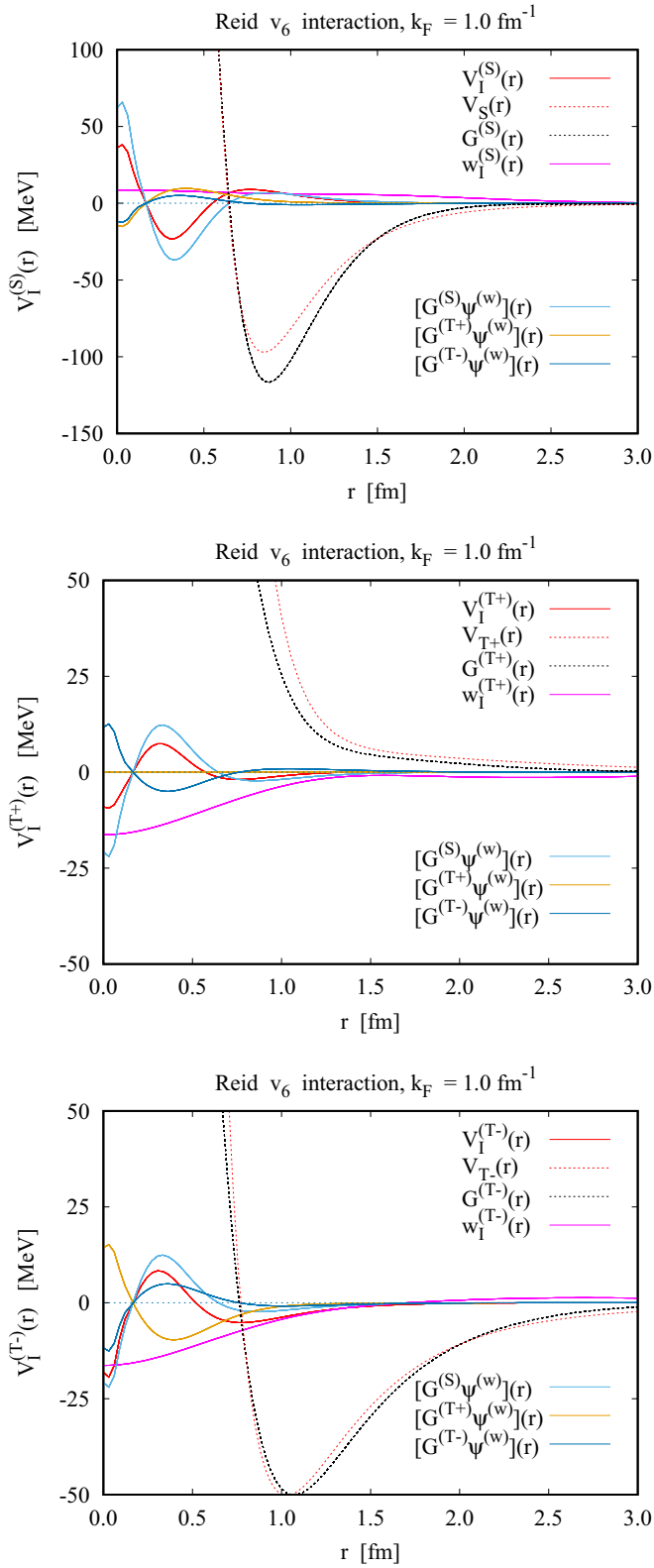

FIG. 7. The figures show, for the Reid v_6 interaction at $k_F = 1.0$ fm^{-1} the "twisted chain" correction $V_I(r)$ (red) to the effective interactions, the induced interaction $w_I(\mathbf{r})$ (dark blue), the G matrix (black dashed) in the local approximation (2.13) and the individual components of $V_I(r)$ (light blue, beige, and dark blue lines) in the projector channels S, $T+$, and $T-$. We also show for reference the bare interaction in the same channels (red dashed lines).

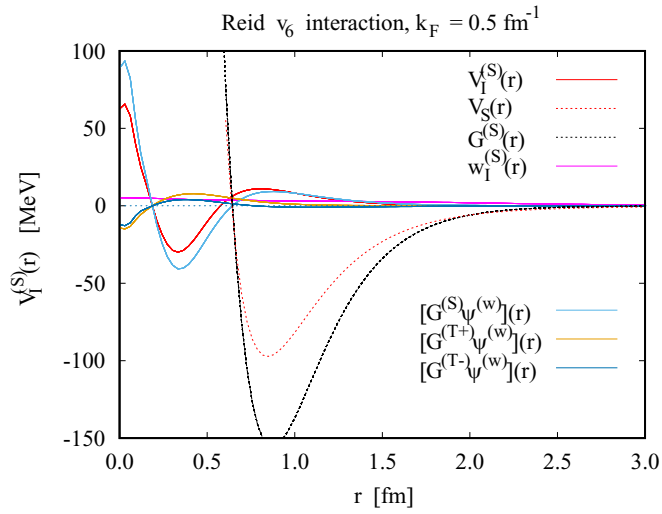

FIG. 8. Same as Fig. 7 for $k_F = 0.5$ fm^{-1}. Only the singlet channel is shown.

The situation changes rather drastically at lower densities. We show in Fig. 8 the individual components of the interaction for $k_F = 0.5$ fm^{-1}. In the singlet channel, the $V_I(r)$ is much larger than the induced interaction $w_I(r)$ and is, therefore, the dominant many-body effect. The G matrix becomes significantly more attractive in the spin-singlet channel. The reason for this is found in the fact that the bare S-wave interaction is, with a scattering length of $a_0 \approx -18.7$ fm [49], rather attractive and close to a bound state. As a consequence, the pair wave function $\psi(r)$ can change substantially if the interaction is only slightly changed, this is the reason for the rather large nearest-neighbor peak seen in Fig. 1. The large nearest-neighbor peak has, in turn, the consequence that the G matrix becomes significantly more attractive than the bare interaction. Of course, many-body effects and the Pauli principles still play the dominant role in determining the pair wave function: The zero-energy S-wave scattering function has a nearest-neighbor peak of about 12, it is therefore nowhere close to the in-medium pair wave function.

On the other hand, the correction from both the induced interaction $\hat{w}_I(r)$ and the "twisted chain" diagrams in the triplet channels is again overwhelmed by the large core size of the bare interaction and therefore not shown.

B. Correlation functions

To document the sensitivity of the pair correlations to the treatment of many-body correlations, we show in Fig. 9 the pair wave function $\psi_\alpha(r)$ in the three channels $\{S, T+, T-\}$. By adding the non-parquet contributions to the irreducible interaction, the peak in the pair wave function is reduced by about 10% . The effect is easily understood by the fact that the irreducible diagrams mix a part of the more repulsive spin-triplet interactions into the spin-singlet channel. The change is visible but much more moderate in the spin-triplet channels which is consistent with our findings on the effective interactions in Figs. 7 and 8. The effect becomes larger at low densities because the attractive induced interaction becomes

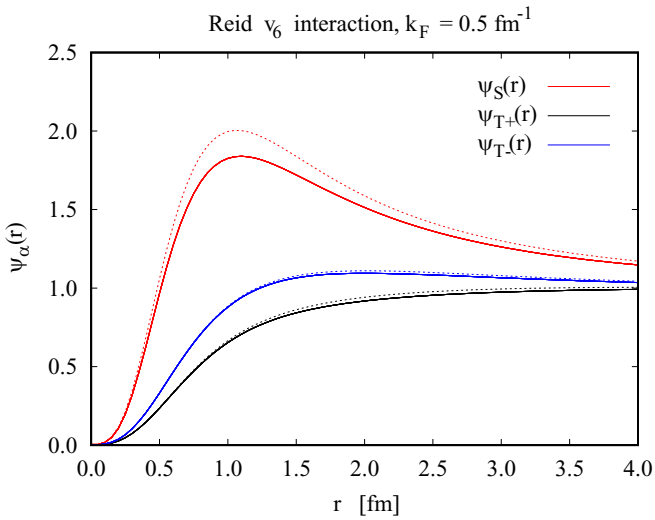

FIG. 9. The figures show, for the Reid v_6 interaction at $k_F = 0.5$ fm^{-1}, the pair wave function $\psi_\alpha(r)$ in the three projector channels S (red), $T+$ (black), and $T-$ (blue). The dashed lines show the parquet//1 case. Each corresponding solid line represents what is obtained if non-parquet diagrams are included.

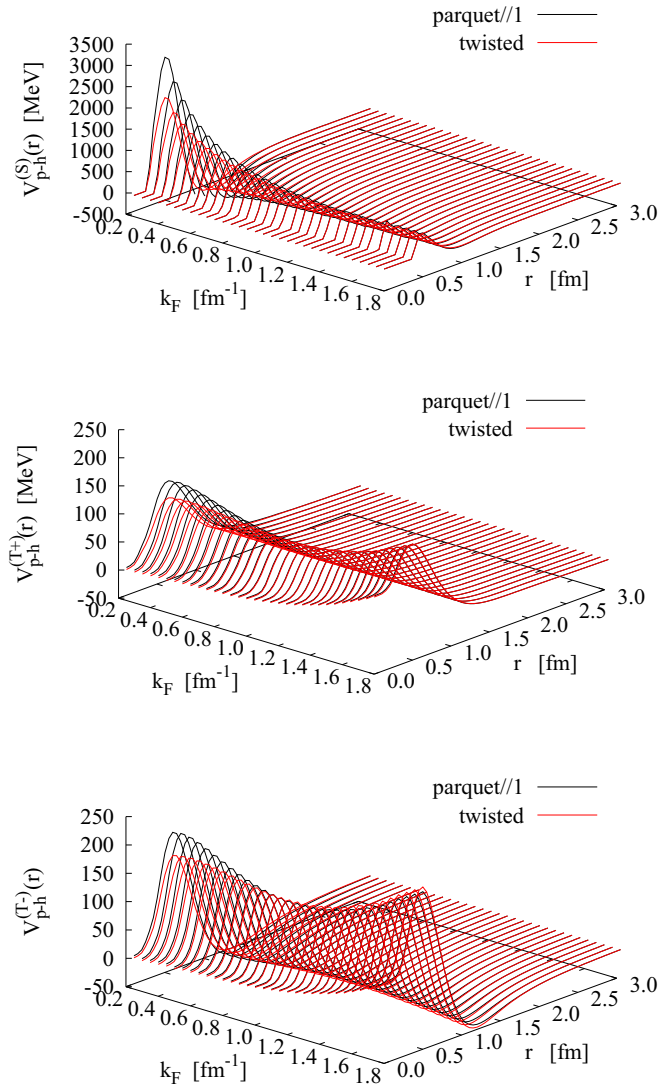

FIG. 10. The figures show, for the Reid v_6 interaction the coordinate-space representation of the particle-hole interaction without (black lines) and with (red lines) the "twisted chain" corrections as a function of the Fermi wave number in the projector channels S, $T+$, and $T-$.

weaker whereas the repulsive non-parquet corrections remain roughly the same.

The strongly attractive S-wave interaction has led to discussions of a potential BCS-BEC crossover in low-density neutron matter [43,50], our findings would suggest that many-body effects can somewhat reduce such a crossover. It must be kept in mind, however, that the repulsive interaction in the spin-triplet channels must not be neglected; it is responsible for stabilizing neutron matter. A model system of nucleons interacting in all channels with the S wave interaction would have a very low density spinodal point and would be unstable at any density that might be of interest for the structure of neutron stars.

C. Effective interactions

Figures 10 shows the full particle-hole interaction in the three projections $\{S, T+, T-\}$ with and without $V_{\rm I}(r)$. The total effect of adding "beyond parquet" corrections is in all three channels a reduction of the short-ranged repulsion; the effect is strongest in the S-channel, this is partly due to the strong nearest-neighbor peak of the pair wave function, see Fig. 1. We also observe a reduction of the attraction between distances of 0.5 and 1 fm. In general we observe that the many-body effects are comparatively weak *despite* the fact that $V_I(r)$ is the dominant effect.

We conclude this section by remarking that the importance of non-parquet diagrams is much less visible in momentum space, this is basically caused by the fact that the long-wavelength limit of both the particle-hole interaction and the induced interaction are determined by Fermi-liquid parameters which come out reasonably well even in the ordinary FHNC-EL or parquet theory.

V. SUMMARY

We have in this paper developed a procedure to go beyond parquet-diagram calculations in a nuclear many-body Hamiltonian. The essential aspect of that Hamiltonian is the state dependence of the interaction. We have analyzed the symmetrized operator product form of the wave function of the type (1.8) and have come to the conclusion that commutator corrections, which have so far been ignored, can massively compromise the vailidity of low-order methods, and can be very important in cases where the interactions in spin-singlet and spin-triplet states are very different. The problem largely removed in parquet theory that can be formulated in terms of physical observables and has no need for introducing variational correlation functions.

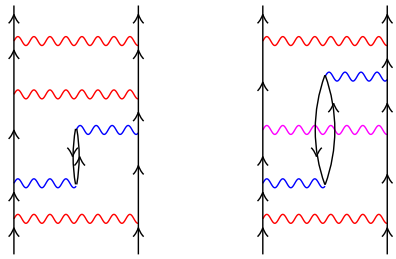

FIG. 11. The figure shows the essential processes are included in the "twisted chain" interaction correction. The red wavy lines are either spin-singlet or spin-triplet interactions, the magenta line may be either of the two, and the blue lines represent the induced interaction $\hat{w}_l$.

The physical mechanism for why this is the case is made clear by looking at the relevant processes from the point of view of diagrammatic perturbation theory. The relevant mechanism is summarized in Fig. 11. In the left diagram, a pair of particles that enter the process in a specific (singlet or triplet) state will always remain in that state. The red wavy lines therefore describe interactions in the *same* channel. This is not changed by the exchange of a spin-fluctuation despite the fact that the blue lines may be singlet or triplet interactions.

In the right diagram, a spin is absorbed, transported through a spin-fluctuation (described by the chain of two blue wavy lines), and reabsorbed at a later time. Therefore, the magenta wavy line may be a triplet interaction whereas the red lines are singlet interactions or vice versa. Evidently, this makes little difference if the interactions are the same in spin-singlet and spin-triplet states. On the other hand, there is no reason that this is a valid approximation if the interactions are very different which is the case for modern nucleon-nucleon interactions [1,4].

On the technical side we have utilized techniques from both variational Jastrow-Feenberg theory and perturbation theory. The analysis of the symmetrized operator product form of the variational wave function has indicated the potential importance of commutator corrections. The correspondence between Jastrow-Feenberg and Goldstone diagrams has then revealed that these commutator corrections correspond to Goldstone diagrams outside the parquet class, it also suggested a way to calculate these corrections that would not be immediately obvious from just looking at, for example, the third diagram in Fig. 4.

To deal with this effect, we have utilized experience from both variational and perturbation theory. We have used the correspondence between Jastrow-Feenberg and Goldstone diagrams to conclude that these processes are not described by parquet diagrams. The practical implementation of these terms utilized again the view of variational wave functions to identify approximations for those non-parquet diagrams that would not be obvious from a purely perturbative point of view.

From the analysis of the commutator diagrams one might have expected a larger effect on the energetics of the system. The reader is reminded that the argument applies only when the correlation functions $f_\alpha(r)$ are determined by some low-order methods *and* commutator corrections are included. We have shown in previous work [34], which is briefly outlined in the Appendix, that this effect can be drastic. FHNC-EL completely eliminates the need for introducing correlation functions $f_\alpha(r)$ and is formulated entirely in terms of the pair distribution function or the direct correlation function $\Gamma_{\rm dd}(r)$, parquet theory never even introduces such correlation functions. That way, the problem of potentially divergent contributions never occurs which can otherwise only be solved by omitting them.

The results have been described in Sec. IV, there is no need for repetition. The effect of the non-parquet contribution on the short-ranged correlations and the effective interactions in the spin-singlet channel at low densities is enhanced by the relatively strong attraction. We have commented on this effect in earlier work [51].

The strong S-wave interaction has led to discussions of a potential BCS-BEC crossover in low-density neutron matter [43,50], our findings would suggest that many-body effects can suppress such a crossover. It must be kept in mind, however, that the repulsive interaction in the spin-triplet channels is responsible for stabilizing neutron matter. A model system of nucleons interacting in all channels with the S wave interaction would have a very low density spinodal point and be unstable at any density that might be of interest for the structure of neutron stars.

We have shown here only the most essential results, namely effective interactions which are input to calculations of pairing phenomena or low-lying excitations. For recent review articles on pairing phenomena, see Refs. [43] or [44] and a collection of papers describing recent research [45]. Most recently [52], we have applied the methods developed here for the calculation of pairing gaps in neutron matter. We found indeed that the corrections arising from the "beyond-parquet" diagrams are important and lead to results that agree quite well with quantum Monte Carlo data [53].

Similarly important is the response of neutron matter which has been discussed over the years [46–48]. A particular promising route appears to be the extension of the pair excitation theory [54,55] to nuclear cases which have provided a quantitative understanding of the full dynamic structure function of quantum fluids [56–58]. The method may be understood as a correlated version of what is called in nuclear physics "second RPA [59–64]," being built on a correlated ground state instead of a model state of single-particle wave functions, the approach avoids the usual problems caused by strong, short-ranged correlations. Another important further extension of our methods is, of course, the inclusion of spin-orbit forces which are of quantitative importance [65]. Work in this direction is in progress.

ACKNOWLEDGMENTS

Encouragement for this work was derived from a workshop on Nuclear Many-Body Theories: Beyond the Mean Field Approaches at the Asia Pacific Center for Theoretical Physics in Pohang, South Korea, in July 2019. J.W. thanks the Austrian Marshall Plan Foundation for support during the summer 2018 and Robert Zillich for discussions.

APPENDIX: A SIMPLE EXAMPLE

We review in this section a somewhat simpler case where the effect of the symmetrization can be studied explicitly. Consider a fictitious system of bosons with spins [34]. We keep only the $\hat{O}_c = \mathbb{1}$ and $\hat{O}_3(i,j) = \boldsymbol{\sigma}_i \cdot \boldsymbol{\sigma}_j$. In that case, the cluster expansions can be simplified by assuming a symmetrized operator product for the *square* of the wave function,

$$\Psi_0^2 = \mathcal{S}\left\{\prod_{i<j}\left[f_c^2(r_{ij}) + f_\sigma^2(r_{ij})\sigma_i \cdot \sigma_j\right]\right\}. \tag{A1}$$

The distribution functions then have the general form

$$\begin{aligned} g_c(r) &= f_c^2(r)F_{cc}(r) + f_\sigma^2(r)F_{c\sigma}(r) \\ g_\sigma(r) &= f_c^2(r)F_{\sigma c}(r) + f_\sigma^2(r)F_{\sigma\sigma}(r). \end{aligned} \tag{A2}$$

where the F_{ij} are multidimensional integrals involving $h_c(r_{ij}) = f_c^2(r_{ij}) - 1$ and $h_\sigma(r_{ij}) = f_\sigma^2(r_{ij})$. If one ignores all commutators, a set of HNC equations can be derived in much the same way as for spin-independent correlations. The coefficient functions $F_{\alpha\beta}(r)$ become

$$\begin{aligned} F_{cc}(r) &= \tfrac{1}{4}[3e^{N_\sigma(r)} + e^{-3N_\sigma(r)}]e^{N_c(r)} \\ F_{c\sigma}(r) &= \tfrac{3}{4}[e^{N_\sigma(r)} - e^{-3N_\sigma(r)}]e^{N_c(r)} = 3F_{\sigma c}(r) \\ F_{\sigma\sigma}(r) &= \tfrac{1}{4}[e^{N_\sigma(r)} + 3e^{-3N_\sigma(r)}]e^{N_c(r)}, \end{aligned} \tag{A3}$$

where the $N_{c,\sigma}(r)$ are the sums of chain diagrams. Defining the sets of nonnodal diagrams

$$X_c(r) = g_c(r) - 1 - N_c(r), \quad X_\sigma(r) = g_\sigma(r) - N_\sigma(r), \tag{A4}$$

the nodal diagrams $N_{c,\sigma}(r)$ are given in momentum space,

$$\tilde{N}_{c,\sigma}(k) = \tilde{X}_{c,\sigma}^2(k)/[1 - \tilde{X}_{c,\sigma}(k)]. \tag{A5}$$

In the next step, the parallel connections of all possible chains are symmetrized with the appropriate combinatorial factors. One then obtains a different set of coupling coefficients [34,66]

$$\begin{aligned} F_{cc}(r) &= [\cosh(N_\sigma(r)) + N_\sigma(r)\sinh(N_\sigma(r))]e^{N_c(r)} \\ F_{c\sigma}(r) &= [2\sinh(N_\sigma(r)) + N_\sigma(r)\cosh(N_\sigma(r))]e^{N_c(r)} \\ &= 3F_{\sigma c}(r) \\ F_{\sigma\sigma}(r) &= \left[\cosh(N_\sigma(r)) + \tfrac{1}{3}N_\sigma(r)\sinh(N_\sigma(r))\right]e^{N_c(r)}. \end{aligned} \tag{A6}$$

Equations (A3) and (A6) look, at the first glance, innocuous. To demonstrate our point we rewrite the pair-distribution functions in the singlet and triplet channels,

$$g(r) = g_s(r)\hat{P}_s + g_t(r)\hat{P}_t, \tag{A7}$$

where

$$g_s(r) = g_c(r) - 3g_\sigma(r), \quad g_t(r) = g_c(r) + g_\sigma(r), \tag{A8}$$

are the distribution functions and nodal quantities in these channels. In this representation we have, for the *unsymmetrized* version (A3)

$$g_{s,t}(r) = f_{s,t}^2(r)e^{N_{s,t}(r)}, \tag{A9}$$

i.e., the distribution functions are indeed proportional to the correlation functions in the spin-singlet and spin-triplet channels. On the other hand, such a simple relationship can not be derived if the simplest nontrivial commutators are included as in Eqs. (A6). The pair distribution functions $g_{s,t}(r)$ are combinations of $f_s^2(r)$ and $f_t^2(r)$ whose detailed structure is not illuminating.

[1] R. V. Reid, Jr., Ann. Phys. (NY) **50**, 411 (1968).
[2] H. A. Bethe and M. B. Johnson, Nucl. Phys. A **230**, 1 (1974).
[3] B. D. Day, Phys. Rev. C **24**, 1203 (1981).
[4] R. B. Wiringa, V. G. J. Stoks, and R. Schiavilla, Phys. Rev. C **51**, 38 (1995).
[5] R. B. Wiringa, R. A. Smith, and T. L. Ainsworth, Phys. Rev. C **29**, 1207 (1984).
[6] B. L. Friman, J. Niskanen, and E. M. Nyman, Nucl. Phys. A **383**, 285 (1982).
[7] E. Feenberg, *Theory of Quantum Fluids* (Academic Press, New York, 1969).
[8] C. W. Woo, Phys. Rev. Lett. **28**, 1442 (1972).
[9] C. W. Woo, Phys. Rev. A **6**, 2312 (1972).
[10] C. C. Chang and C. E. Campbell, Phys. Rev. B **13**, 3779 (1976).
[11] E. Krotscheck, Phys. Rev. B **33**, 3158 (1986).
[12] E. Krotscheck, J. Low Temp. Phys. **119**, 103 (2000).
[13] M. Kalos, D. Levesque, and L. Verlet, Phys. Rev. A **9**, 2178 (1974).
[14] D. M. Ceperley, Phys. Rev. B **18**, 3126 (1978).
[15] D. M. Ceperley, Rev. Mod. Phys. **67**, 279 (1995).
[16] J. Boronat, in *Microscopic Approaches to Quantum Liquids in Confined Geometries*, edited by E. Krotscheck and J. Navarro (World Scientific, Singapore, 2002), pp. 21–90.
[17] J. M. J. van Leeuwen, J. Groeneveld, and J. D. Boer, Physica **25**, 792 (1959).
[18] H. K. Sim, C.-W. Woo, and J. R. Buchler, Phys. Rev. A **2**, 2024 (1970).
[19] A. D. Jackson, A. Lande, and R. A. Smith, Phys. Rep. **86**, 55 (1982).
[20] A. D. Jackson, A. Lande, and R. A. Smith, Phys. Rev. Lett. **54**, 1469 (1985).
[21] E. Krotscheck, R. A. Smith, and A. D. Jackson, Phys. Rev. A **33**, 3535 (1986).
[22] E. Krotscheck, Phys. Rev. A **15**, 397 (1977).
[23] S. Fantoni and S. Rosati, Nuovo Cimento A **43**, 413 (1978).
[24] V. R. Pandharipande and R. B. Wiringa, Rev. Mod. Phys. **51**, 821 (1979).
[25] E. Krotscheck, Phys. Lett. A **190**, 201 (1994).
[26] R. F. Bishop, in *Condensed Matter Theories*, edited by M. Casas, J. Navarro, and A. Polls (Nova Science Publishers, Commack, NY, 1995), Vol. 10, pp. 483–508.
[27] B. L. Scott and S. A. Moszkowski, Nucl. Phys. **29**, 665 (1962).
[28] V. R. Pandharipande and H. A. Bethe, Phys. Rev. C **7**, 1312 (1973).
[29] J. C. Owen, R. F. Bishop, and J. M. Irvine, Nucl. Phys. A **274**, 108 (1976).

[30] S. A. Moszkowski and B. L. Scott, Ann. Phys. **11**, 65 (1960).
[31] T. Ohmura, Prog. Theor. Phys. **41**, 419 (1969).
[32] R. A. Smith and A. D. Jackson, Nucl. Phys. A **476**, 448 (1988).
[33] E. Krotscheck and J. Wang, Phys. Rev. C **101**, 065804 (2020).
[34] E. Krotscheck, Nucl. Phys. A **482**, 617 (1988).
[35] H. A. Bethe and J. Goldstone, Proc. R. Soc. Lond. Ser. A **238**, 551 (1957).
[36] A. L. Fetter and J. D. Walecka, *Quantum Theory of Many-Particle Systems* (McGraw–Hill, New York, 1971).
[37] S. Shlomo, V. M. Kolomietz, and G. Colò, Eur. Phys. J. A **30**, 23 (2006).
[38] D. N. Lowy and G. E. Brown, Phys. Rev. B **12**, 2138 (1975).
[39] H.-H. Fan and E. Krotscheck, Phys. Rep. **823**, 1 (2019).
[40] M. Gaudin, J. Gillespie, and G. Ripka, Nucl. Phys. A **176**, 237 (1971).
[41] G. Ripka, Nucl. Phys. A **314**, 115 (1979).
[42] J. W. Clark, in *Progress in Particle and Nuclear Physics*, edited by D. H. Wilkinson (Pergamon Press, Oxford, 1979), Vol. 2, pp. 89–199.
[43] G. C. Strinati, P. Pieri, G. Roepke, P. Schuck, and M. Urban, Phys. Rep. **738**, 1 (2018).
[44] A. Sedrakian and J. W. Clark, Eur. Phys. J. A **55**, 167 (2019).
[45] *Pairing and Condensation in Fermionic Systems*, edited by E. Krotscheck, J. Low Temp. Phys., Vol. 189 (Springer, New York, 2017).
[46] J. Wambach, T. Ainsworth, and D. Pines, Nucl. Phys. A **555**, 128 (1993).
[47] O. Benhar and N. Farina, Phys. Lett. B **680**, 305 (2009).
[48] A. Lovato, C. Losa, and O. Benhar, Nucl. Phys. A **901**, 22 (2013).
[49] D. E. González Trotter, F. Salinas, Q. Chen, A. S. Crowell, W. Glöckle, C. R. Howell, C. D. Roper, D. Schmidt, I. Šlaus, H. Tang, W. Tornow, R. L. Walter, H. Witała, and Z. Zhou, Phys. Rev. Lett. **83**, 3788 (1999).
[50] M. Stein, A. Sedrakian, X.-G. Huang, and J. W. Clark, Phys. Rev. C **90**, 065804 (2014).
[51] E. Krotscheck and J. Wang, Phys. Lett. B **809**, 135770 (2020).
[52] E. Krotscheck and J. Wang, arXiv:2009.10849.
[53] A. Gezerlis and J. Carlson, Phys. Rev. C **77**, 032801(R) (2008).
[54] C. E. Campbell, E. Krotscheck, and T. Lichtenegger, Phys. Rev. B **91**, 184510 (2015).
[55] H. M. Böhm, R. Holler, E. Krotscheck, and M. Panholzer, Phys. Rev. B **82**, 224505 (2010).
[56] H. Godfrin, M. Meschke, H.-J. Lauter, A. Sultan, H. M. Böhm, E. Krotscheck, and M. Panholzer, Nature **483**, 576 (2012).
[57] K. Beauvois, J. Dawidowski, B. Fåk, H. Godfrin, E. Krotscheck, J. Ollivier, and A. Sultan, Phys. Rev. B **97**, 184520 (2018).
[58] T. Lichtenegger, Spin-Density Fluctuations in Liquid ^{3}He, Ph.D. thesis, Johannes Kepler Universität Linz, 2013.
[59] J. Sawicki, Phys. Rev. **126**, 2231 (1962).
[60] J. da Providencia, Nucl. Phys. A **161**, 87 (1965).
[61] C. Yannouleas, M. Dworzecka, and J. J. Griffin, Nucl. Phys. A **397**, 239 (1983).
[62] C. Yannouleas, Phys. Rev. C **35**, 1159 (1987).
[63] J. Wambach, Rep. Prog. Phys. **51**, 989 (1988).
[64] P. Papakonstantinou and R. Roth, Phys. Rev. C **81**, 024317 (2010).
[65] I. Bombaci, A. Fabrocini, A. Polls, and I. Vidana, Phys. Lett. B **609**, 232 (2005).
[66] I. Lagaris, Anales de Fisica **81**, 39 (1985).